Supplementary Material for "Even-odd product variation of the $C_n^+ + D_2$ (n=4-9) reaction: Complexity of the linear carbon cation electronic states"

Kiichirou Koyasu[a+], Tomohiro Ohtaki[a], Bing Jin[b], Kaito Takahashi[b]*, and Fuminori Misaizu[a*]

a) Department of Chemistry, Graduate School of Science, Tohoku University, Aramaki-Aoba, Aoba-ku, Sendai 980-8578, Japan

b) Institute of Atomic and Molecular Sciences, Academia Sinica, P.O.Box 23-166, Taipei,10617 Taiwan R. O. C.

+) Present address: Department of Chemistry, School of Science, The University of Tokyo, 7–3–1 Hongo, Bunkyo-ku, Tokyo 113–0033, Japan

***FM: Tel +81 22 – 795 – 6577, Email: misaizu@m.tohoku.ac.jp ;**

***KT: Tel+886-223668237, Email: kt@gate.sinica.edu.tw**

Details concerning the experimental results, details on the quantum chemistry calculation of reactants and products, and details concerning the potential energy surface calculation are given in the supplementary material. Figures of the ion spectrum of C_n^+, D adduct, D_2 adduct; comparison of reactivity of linear and cyclic C_9^+ chains; molecular orbitals for C_n^+ (n=4-9) as well as the stable geometries of the C_n^+, C_nD^+ $C_nD_2^+$, and DC_nD^+ are given in the supplementary materials. Tables of the relative

energies of C_n^+, C_nD^+ $C_nD_2^+$, and DC_nD, the frequencies for the D_2 adducts, and comparison on the dissociation energy of the products; as well as full reference 33 are available in the supplementary material.

Detailed method to experimentally obtain the collision cross section:

The ion mobility K was obtained under the number of density N at the experimental condition. In order to compare this with results obtained at different conditions, K was corrected to the reduced ion mobility at the standard condition, K_0. The formula for the calculation is expressed as follow,

$$K_0 = \frac{N}{N_0} K = \frac{T_0}{T} \frac{p}{p_0} K. \qquad \text{(S1)},$$

where T_0 = 273.15 K and p_0 = 760 Torr.

Then, collision cross section, Ω, was estimated by using eq. S1 in order to obtain collision numbers of target ion in the drift cell;[1]

$$\Omega = \frac{3e}{16N_0} \sqrt{\frac{2\pi}{k_B \mu T_{eff}}} \frac{1}{K_0} \qquad \text{(S1)},$$

where e, N_0, k_B, μ, T_{eff}, K_0 respectively represent element charge, number density at the standard condition (pressure: 101325 Pa and temperature: 273.15 K), the Boltzmann constant, a reduced mass of target ion and buffer gas (He), an effective temperature, and a reduced ion mobility.

For example, K_0 of C_9^+ was 9.671 × 10^{-4} m^2 V^{-1} s^{-1}, and then of Ω of C_9^+ was 47.02 $Å^2$.

Detailed method to fit the experimentally obtained intensity:

Decay of C_n^+ intensity and growth of intensities of C_nD^+ and $C_nD_2^+$ were fitted by the following formula;

Decay: $[C_n^+(t)] = [C_n^+(t = 0)] \exp(-A [D_2] t)$ (S2)

Growth: $[C_nD^+(t)] = [C_n^+(t = 0)] B \{1 - \exp(-C [D_2] t)\}$ (S3)

Detailed discussion on experimental results:

As shown in Fig. S1, using the time of flight mass spectra, we can quantify the reactants and products. The peaks for the parent, and single/double D adducts can be seen clearly in the figures. From the D_2 concentration dependence of the signal for isomer selected C_9^+ given in Fig. S2, we can quantify that the linear species react while the cyclic do not.

Detailed discussion and convergence tests for the quantum chemistry calculation:

All the ROHF-UCCSD(T)/cc-pVTZ energies for C_n^+ are given in Tables S1 and S2. The geometries of the two lowest electronic states are given in Fig. S3. To test the basis set dependence we also performed ROHF-UCCSD(T) optimization using the cc-pVDZ and cc-pVQZ basis sets for the symmetry broken $^2\Sigma$ and $^2\Sigma_g$, $^2\Sigma_u$, and $^2\Pi_{g/u}$ states for the odd chains. Other than the C_5^+ chain using cc-pVDZ, all other calculation converged to a symmetry broken solution. Previously, Schnell et al.[2] proposed that the symmetry broken solution was an artifact because geometries for the C_5^+ using CCSD(T) method converged to symmetric geometries, but we suspect that this may be due to the use of the small cc-pVDZ basis. We also performed frequency calculation to confirm that the linear geometries were a stable minimum for the $^2\Pi_{g/u}$ for the even chains and $^2\Sigma$, $^2\Sigma_{g/u}$ and $^2\Pi_{g/u}$ for the odd chains using the ROHF-UCCSD(T)/cc-pVTZ method. Only the C_5^+ $^2\Pi_g$, C_7^+ $^2\Sigma_g$, and C_9^+ $^2\Sigma_{g/u}$ states showed small imaginary frequencies to bend the chain as given in Table S3. Thereby, we conclude that within the approximation for ROHF-UCCSD(T) method the symmetry broken $^2\Sigma$ ($^4\Sigma$) states are the ground state or lie close in energy with the $^2\Pi_{g/u}$ states. We note here that for

odd chains the $^2\Pi$ and $^2\Sigma$ states are close in energy and this can be rationalized from the simple counting methods given previously by Mulliken[3], and Pitzer and Clementi[4]. For a C_n^+ cluster, there are $n - 1$ sigma bonds and 2 edge σ lone pair orbitals in which $2n + 2$ electrons can fill. Since there are $4n - 1$ valance electrons in C_n^+, $2n - 3$ are left to fill the remaining π orbitals. When n is even ($n = 2m$, $m = 1, 2\ldots$) there are $4m - 3$ electrons or one unpaired excess π electron, while for odd ($n = 2m + 1$, $m = 1, 2\ldots$) there are $4m - 1$ electrons or one hole in the π orbital. Thus $^2\sum_{g/u}$ state for odd chains can be generated by moving one electron from the σ orbital to the single occupied π to make a closed Π configuration (see Supplementary Fig. S5, 7, 9). This is not possible for even C_n^+, and rather a $^4\Sigma_{g/u}$ state is found to be lying low in energy to make a half filled Π configuration (see Supplementary Fig S3).

As previously discussed by several groups[5], the broken symmetry solution may be an artifact due to the use of ROHF based correlation methods. It depends on the competition of resonance effects, orbital sizing effect, and vibronic coupling, thus, requires multireference methods such as multiconfigurational self-consistent field method and multi reference configuration interaction (MRCI) method to clarify whether this is real or an artifact of our calculation method. Previous density functional theory studies by Giuffreda et al.[6] have mentioned the possibility of the symmetry broken $C_{\infty v}$ Σ state being lower in energy for the odd species. As mentioned by Orlova and Goddard[7] for linear C_n^+, vibronic coupling of two nearly degerate electronic states Σ_g and Σ_u can split when the $D_{\infty h}$ symmetry is lowered to $C_{\infty v}$ since at this symmetry both states belong to the same Σ symmetry representation. This type of vibronic coupling termed pseudo Jahn-Teller interactions have been seen for larger cyclic carbon

chains and other molecules such as C_3H_3, LiO_2, and NO_3.[5] In the present case, the $^2\Sigma_g$ and $^2\Sigma_u$ states differ by whether the radical spin is in the highest σ_g or σ_u orbital which corresponds to the symmetric and asymmetric combination of the edge σ orbitals (see Figures S4-9). One can easily imagine that as the chain length is elongated the energy difference between these two molecular orbitals will decrease and thus the energy difference between these two electronic states will decrease. As can be seen from Table S1 and S2, as the *n* gets larger the energy difference between $^2\Sigma_u$ and $^2\Sigma_g$ ($^4\Sigma_u$ and $^4\Sigma_g$) decreased for odd (even) chains. Thereby stabilization by vibronic coupling induced symmetry breaking is stronger for the larger clusters. We do note that for the odd $^2\Sigma_{g/u}$ states we obtained unphysical harmonic frequencies of ~ 3300 cm^{-1} for the symmetry breaking CC stretching mode which is usually seen in the 2100 cm^{-1} region signifying that these calculation results should be used with caution as mentioned by Belau et al.[8] In addition the energy difference between the Σ_g and Σ_u structures is ~0.3 eV (~2400 cm^{-1}) much less than the zero point vibration energies of the odd carbon chain cations (4200, 5700 and 8000 cm^{-1} for C_5^+, C_7^+, and C_9^+, respectively), thus the nuclear quantum effects must also have to be considered to confirm the existence of the symmetry broken solutions. However we note that for C_3^+ Crawford and coworkers used equation of motion ionization coupled cluster methods (EOM-IP-CCSD) and found that when constraint to a linear form, C_3^+ favors the symmetry broken solution. Our preliminary calculation using the EOM-IP-CCSD and MRCI has shown that the symmetry broken $^2\Sigma$ state solutions have lower energies than the symmetric $^2\Pi$ states for the odd chains *n*=7,9. In Figure S10, we present the single occupied molecular orbitals of the symmetry broken $^2\Sigma$ state C_5^+, C_7^+, and C_9^+. One can clearly notice that this orbital has large density protruding out of the terminal carbon. To estimate the

degree of protrusion we have performed Atoms In Molecules[9] calculation with B3LYP and obtained the atomic dipole $\vec{\mu}^{\mathrm{ad}}(\vec{R})$ given as

$$\vec{\mu}^{\mathrm{ad}}(\vec{R}) \;=\; -\sum_{\alpha}^{Natom}\int_{V_\alpha}\rho(\vec{r}_\alpha;\vec{R})\,\vec{r}_a\,d\vec{r}_\alpha \;=\; \sum_{\alpha}^{Natom}\vec{\mu}_\alpha^{\mathrm{ad}}(\vec{R}),$$

where $\rho(\vec{r}_\alpha;\vec{R})$ is the electron density at a position vector $\vec{r}_\alpha$ with respect to nucleus α at $\vec{R}_\alpha$. This portion describes the contribution from the shift of the electron position expectation value from the nuclear center. For systems with lone pairs sticking out in a certain direction this atomic dipole contribution is large for that direction. The atomic dipole for the terminal carbon for the symmetry broken $^2\Sigma$ state C_5^+, C_7^+, and C_9^+ were calculated to be -0.26, -0.19, and -0.13 Debye, respectively. Therefore we can understand that the decrease in reactivity with increasing *n* is due to the weakening of the dipolar interaction of the terminal carbon with D_2 for the odd radical abstraction reaction: $C_n^+ + D_2 \rightarrow C_nD^+ + D$. This is consistent with the previous notion that increase in *n* causes the radical electron to delocalize thus making the protrusion of the electron density of the single occupied orbital to decrease.

Detailed discussion on the quantum chemistry calculation for products:

The geometry of the products for the reaction are given in Figures S11-S13. The relative energies for the products, C_nD^+, $C_nD_2^+$, and DC_nD^+ are given in Tables S4, S5, and S6, respectively (in the following theory session we will distinguish the single sided D_2 adduct of C_n^+, shown in supplementary Figure S12, and the acetylene like double sided D_2 adduct of C_n^+, shown in supplementary Figure S13, using the symbols $C_nD_2^+$ and DC_nD^+, respectively). For the single D-atom adduct, C_nD^+, we can predict from the isoelectronic neutral carbon clusters that the most stable electronic state for odd C_n^+ are

singlet while that for even chains are triplet. We also note that, based on the heat of reactions, only the $^1\Sigma$ state is likely to be formed for the odd chains, while all $^1\Sigma$, $^3\Sigma$, and $^3\Pi$ states can be formed for the even chains.

Structure of double D adduct can be shown as single-sided adduct, $C_nD_2^+$, or double-sided adduct, DC_nD^+. Both of their doublet states were calculated to be much more stable than the quartet states. We note here that from the mass and collision cross section itself it is difficult to distinguish $C_nD_2^+$ and DC_nD^+. The calculated harmonic frequencies for the CD stretching vibration for DC_nD^+ (~2600 cm^{-1}) and $C_nD_2^+$ (2300 cm^{-1}) have a 300 cm^{-1} difference. Thereby, infrared vibrational predissociation spectroscopy or multiphoton dissociation heating the CD bond, following the formation of this ion can be performed to confirm which isomer is formed. To aid future studies, the calculated harmonic frequencies and intensities by B3LYP/cc-pVTZ for the most stable conformers are given in the supplementary information Table S7-S12.

For the DC_nD^+ carbon chains, Maier et al.[10] have measured the electronic spectra and report 2.44, 2.48, 2.05, 2.08, 1.73, and 1.78 eV for the lowest energy transition for n = 4, 5, 6, 7, 8, and 9, respectively. We obtain 2.52, 3.46, 2.19, 2.64, 1.89, and 2.49 eV for the lowest energy transition between the Π_g Π_u states for n = 4, 5, 6, 7, 8, and 9, respectively. While for the even chains, the theoretical values closely match the experimental values, the odd theoretical results are overestimated by 0.6 to 1. eV. From the frequency calculation for these DC_nD+ linear chains it was calculated that the Π_g states of DC_5D^+ and DC_9D^+, and Π_u state of DC_7D^+ are not stable minima and have a lower energy isomer by bending the linear chain. We believe that this is the origin of the overestimated transition energy for the odd chain, but since the detailed determination

of the electronic spectra is not the main goal of the present paper we will leave further study on this discrepancy to future work.

Concerning the fragmentation process after the products are formed, as can be seen from Table S13, the C_3 loss channel for $C_nD_2^+$ requires about 5.5 eV while the exothermicity of the $C_n^+ + D_2$ reaction forming $C_nD_2^+$ is about 4.5 eV for these longer chains, thereby an excess of 1 eV collision energy is required for the C_3 loss channel to show up in the $C_n^+ + D_2 \rightarrow C_nD_2^+$ reaction. In addition, for the C_nD^+ forming channel, the C_3 loss channel for $C_nD_2^+$ requires 4.5 eV, however the exothermicity of the $C_n^+ + D_2 \rightarrow C_nD^+ + D$ is about 1.5 eV. As a conclusion more than 3 eV is required in the collision energy. Thereby we think that such process is absent in our experimental set up at room temperature giving at most 0.1 eV of collision energy.

Detailed discussion on the potential energy surface calculation:

In the calculation for the perpendicular approach potential energy surface (Fig S14 and S15), 13 grid points for DD distance (0.6 to 2.6 Å in grids of 0.2 Å; along with 0.74, and 1.9 which corresponds to the equilibrium bond length for D_2 and $C_nD_2^+$), 22 grid points for RCX (0.4 to 2.4 Å in grids of 0.1 Å; along with 0.54 Å which corresponds to the equilibrium distance for $C_nD_2^+$), and 10 grid points for θ (0 to 90 degrees in grids of 10 degrees) were employed. In the calculation for the parallel approach potential energy surface (Fig S16, and S17), 12 grid points for DD distance (0.6 to 1.6 Å in grids of 0.1 Å ; along with 0.74 which corresponds to the equilibrium bond length for D_2), 12 grid points for RCD (0.8 to 1.8 Å in grids of 0.1 Å; along with 1.07 Å which corresponds to the equilibrium distance for C_nD^+), and 10 grid points for θ (0 to 90 degrees in grids of 10 degrees) were employed. All the effective potential energy surface calculations were done using the B3LYP/cc-pVTZ method. It can be seen that the general

trend for the even species are given by the C_4^+ results and that for the odd can be given by the C_5^+ results.

Using the calculated potential energy surface for B3LYP/cc-pVTZ, we determined the effective reaction path by optimizing RDD and θ at a fixed RCX and RCD for the perpendicular, and parallel approach, respectively. In Figure S18, we plot the values of the optimum RDD, θ and energy for the perpendicular approach. As can be seen from Fig S18 (b) the angle has a sudden jump at RCX=1.3 Å, where it changes from sideways (θ~80º) to direct head on (θ~0º). The potential energy surface along this coordinate is all attractive for the B3LYP calculation. In Figure S19, we plot the values of the optimum RDD, θ, and energy for the parallel approach. For the even chains similar to the case in the perpendicular approach, a sideways (θ=80˚) approach is favored until RCD=1.3 Å and at RCD < 1.3 Å, θ=0˚ is favored. When one compares the potential energy curve of the perpendicular and parallel approach for even chains (Figs S18(a) and S19(a)), one can clearly notice that the attractive potential for the parallel approach is much weaker than in the case of the perpendicular approach. Thereby, for the even $^2\Pi$ state the reaction is favored to take the perpendicular approach. On the other hand, for the odd chains, a barrier less encounter is favored along θ=0˚ for parallel approach (Fig S19 (b)). Once RCD approaches 1.5 Å, RDD start elongating without any barriers and a smooth elongation of the D–D bond causes formation of C_5D^++D.

Using the above results from the B3LYP calculation, we also calculated the effective potential energy curve using CCSD(T) method. For the perpendicular approach with θ fixed at 80 degrees, we calculated 12 grid points for RCX (2.4 to 1.3 Angstrom in grids of 0.1 Angstrom) while allowing the RDD to be optimized. Then for θ fixed at 0 degrees, we calculated 10 grid points for RCX (1.25 to 0.35 Angstrom in grids of 0.1 Angstrom) while allowing the RDD to be optimized. For the parallel approach, we fixed θ to be equal to 0 and

calculated 25 grid points for RCD (0.57 to 2.97 Angstrom in grids of 0.1 Angstrom) while allowing the RDD to be optimized for the odd chains with $^2\Sigma$.

Full Reference for 33

33: MOLPRO is a package of ab initio programs written by H.-J. Werner, P. J. Knowles, F. R. Manby, M. Schütz, P. Celani, G. Knizia, T. Korona, R. Lindh, A. Mitrushenkov, G. Rauhut, T. B. Adler, R. D. Amos, A. Bernhardsson, A. Berning, D. L. Cooper, M. J. O. Deegan, A. J. Dobbyn, F. Eckert, E. Goll, C. Hampel, A. Hesselmann, G. Hetzer, T. Hrenar, G. Jansen, C. Köppl, Y. Liu, A. W. Lloyd, R. A. Mata, A. J. May, S. J. McNicholas, W. Meyer, M. E. Mura, A. Nicklaß, P. Palmieri, K. Pflüger, R. Pitzer, M. Reiher, T. Shiozaki, H. Stoll, A. J. Stone, R. Tarroni, T. Thorsteinsson and M. Wang, A. Wolf, *MOLPRO,* version 2010.1, a package of ab initio programs, see http://www.mopro.net.

Figures:

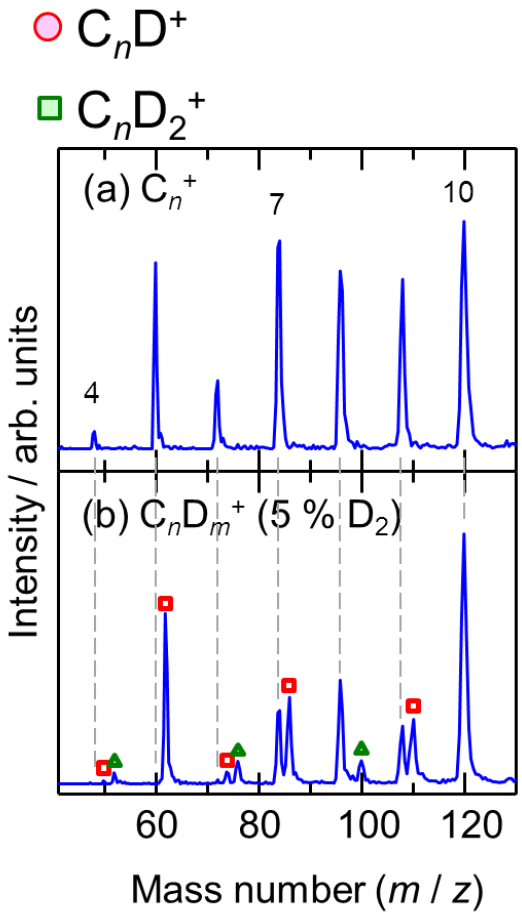

Figure S1: Mass ion spectrum with and without D_2 in the draft chamber.

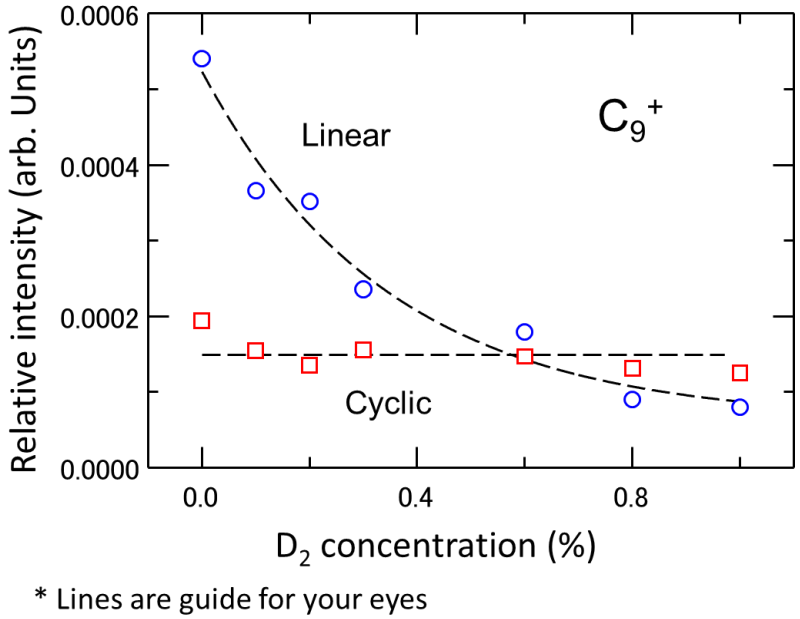

Figure S2: Comparison of reactivity of the linear and cyclic C_n^+

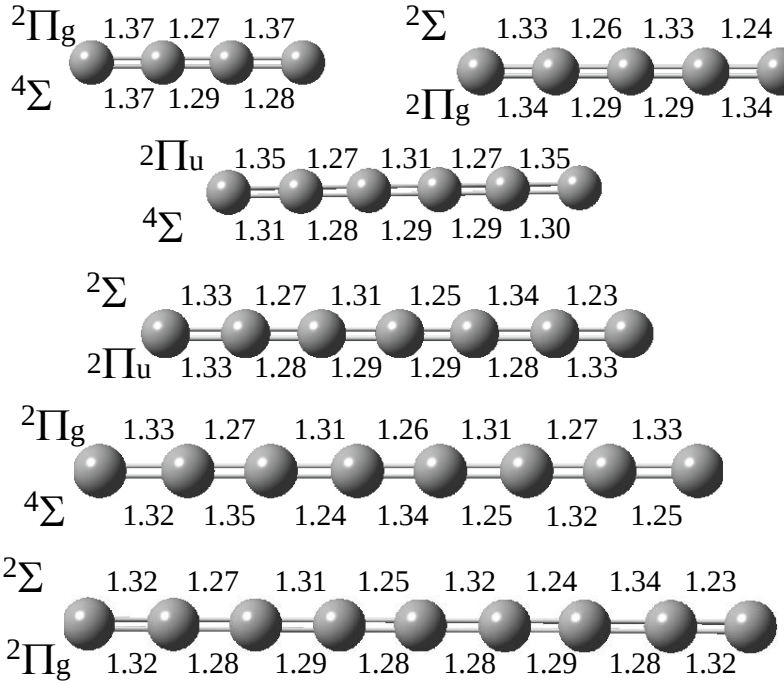

Figure S3: Optimized geometry for the two stable electronic states for linear C_n^+ (n = 4–9)

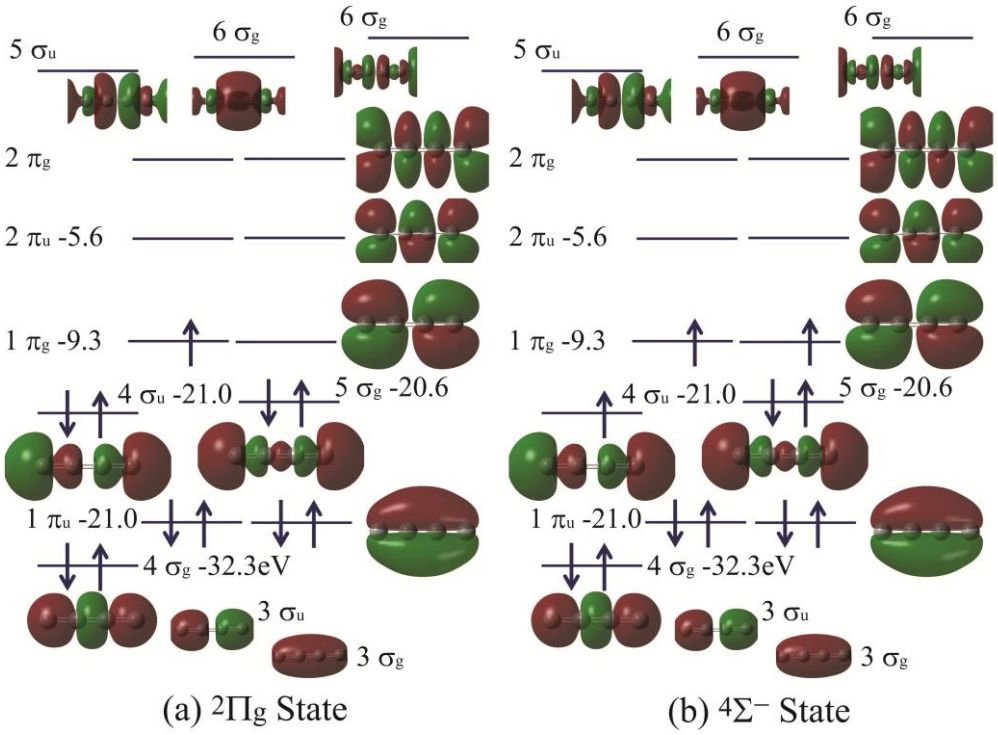

Figure S4: Schematic plot of the molecular orbitals in (a) $^2\Pi_g$ and (b) $^4\Sigma$ of C_4^+

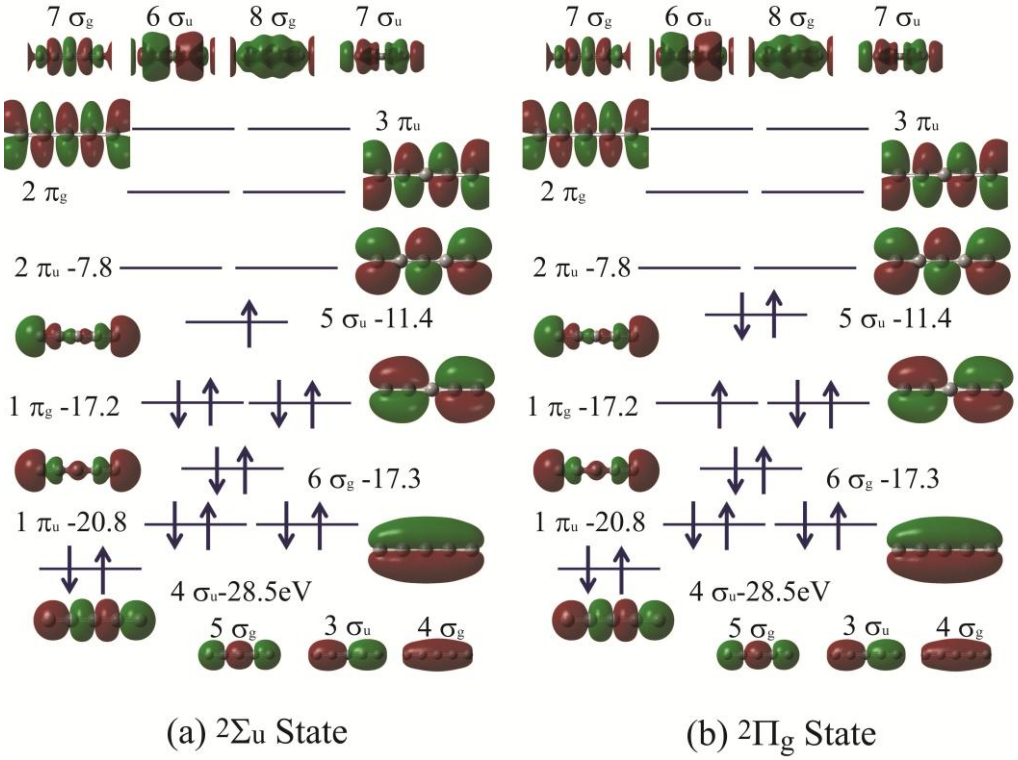

Figure S5: Schematic plot of the molecular orbitals in (a) $^2\Sigma_u$ and (b) $^2\Pi_g$ of C_5^+

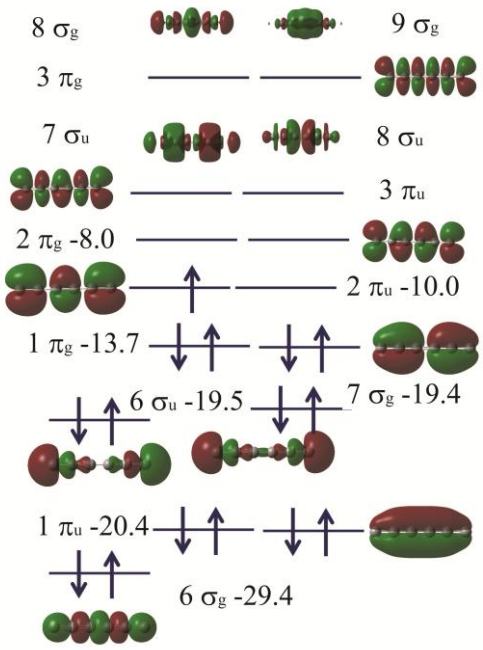

Figure S6: Schematic plot of the molecular orbitals in $^2\Pi_u$ state C_6^+

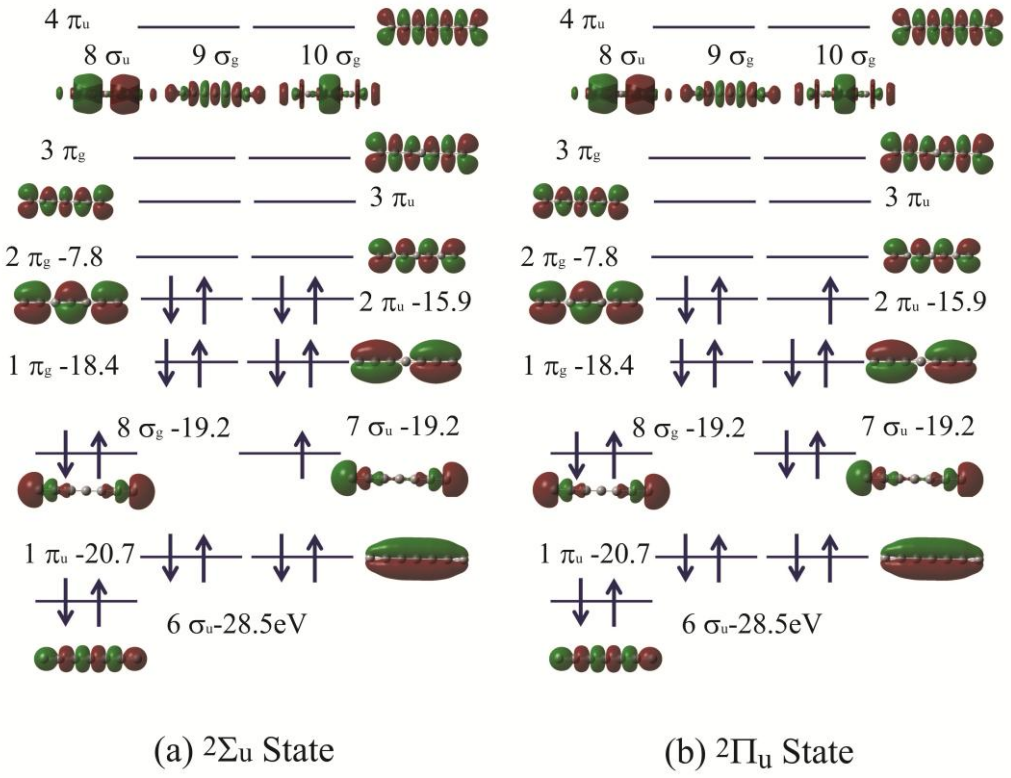

Figure S7: Schematic plot of the molecular orbitals in (a) $^2\Sigma_u$ and (b) $^2\Pi_u$ state of C_7^+

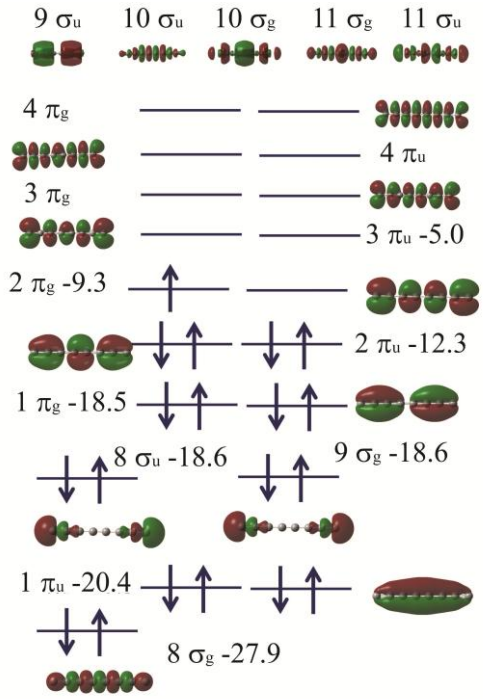

Figure S8: Schematic plot of the molecular orbitals for $^2\Pi_g$ state C_8^+

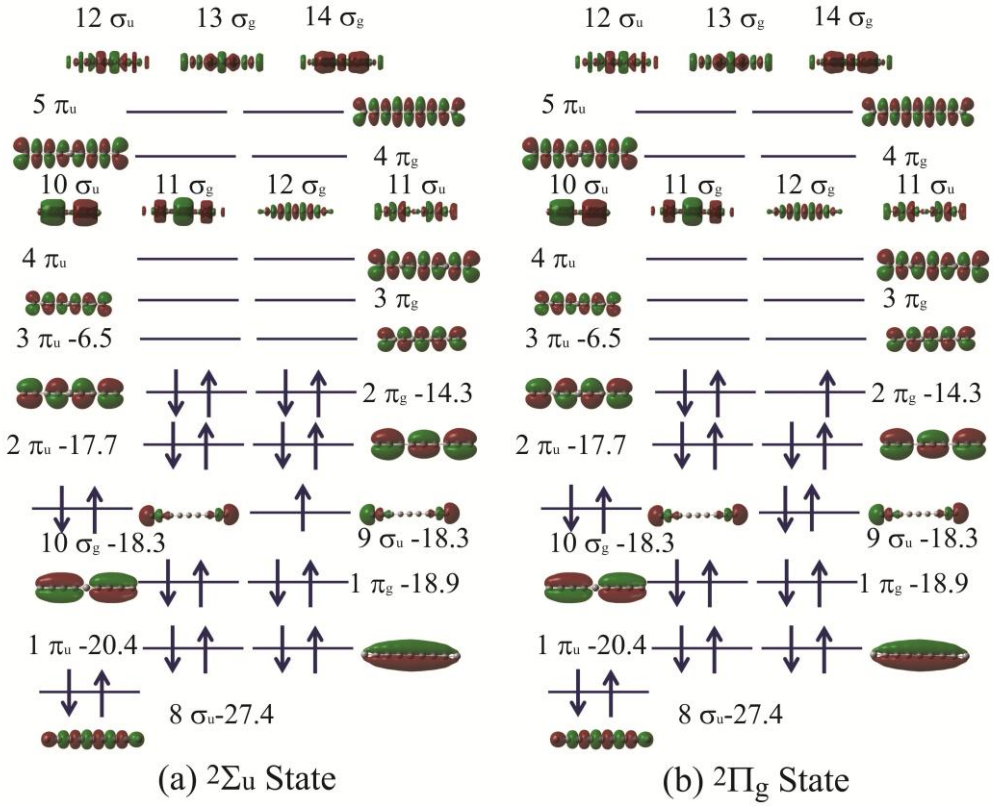

Figure S9: Schematic plot of the molecular orbitals for (a) $^2\Sigma_u$ and (b) $^2\Pi_g$ state C_9^+

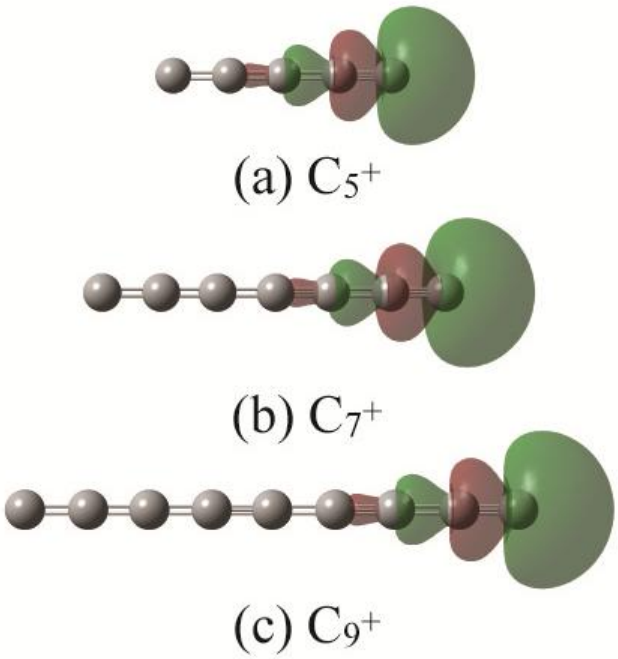

Figure S10: Schematic plot of the single occupied molecular orbitals for the symmetry broken $^2\Sigma$ for (a) C_5^+ (b) C_7^+ and (c) C_9^+

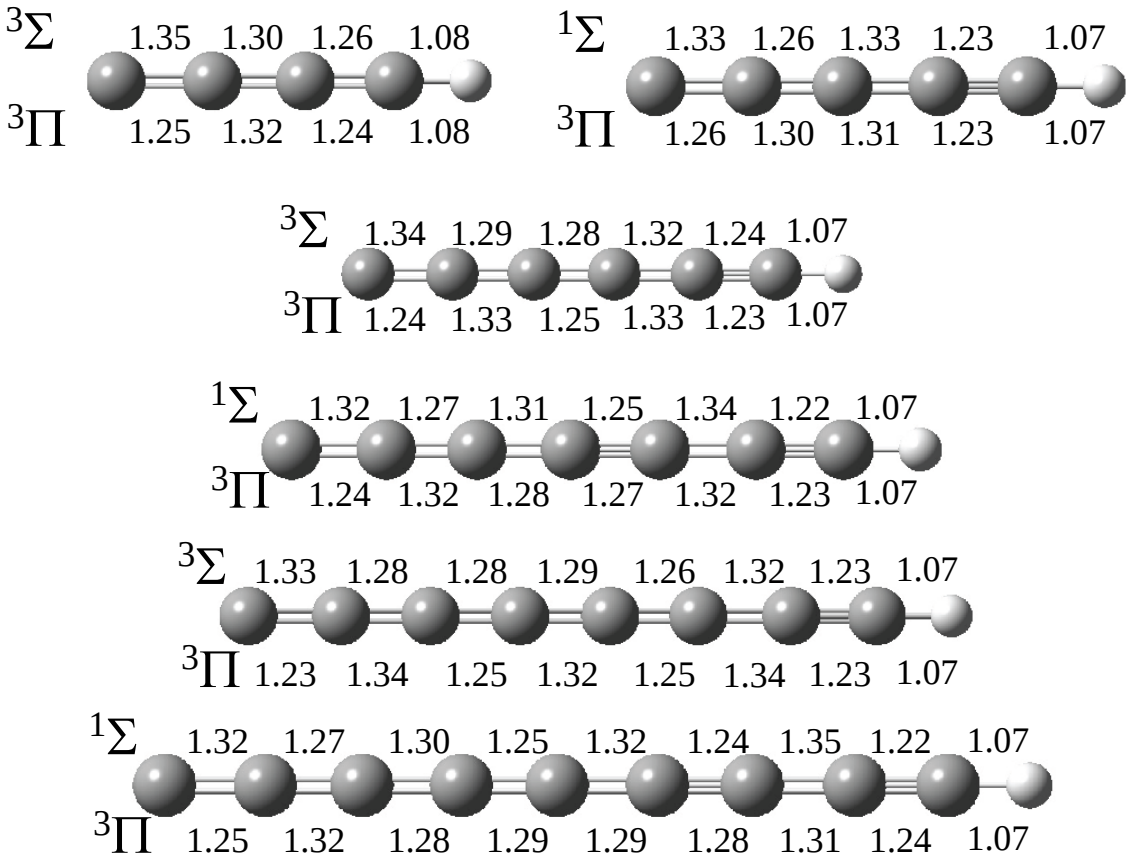

Figure S11: Optimized geometry for the two stable electronic states for linear C_nH^+ (n = 4–9).

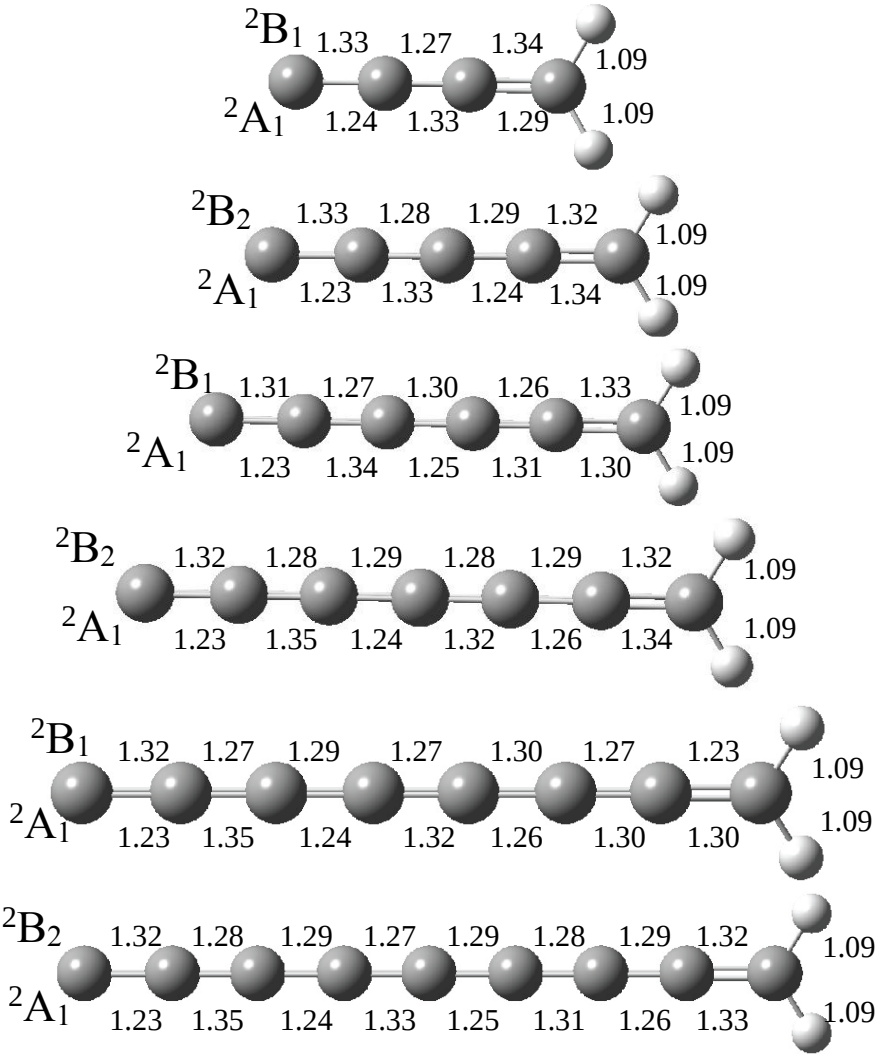

Figure S12: Optimized geometry for the two stable electronic states for linear $C_nH_2^+$ (*n* = 4–9).

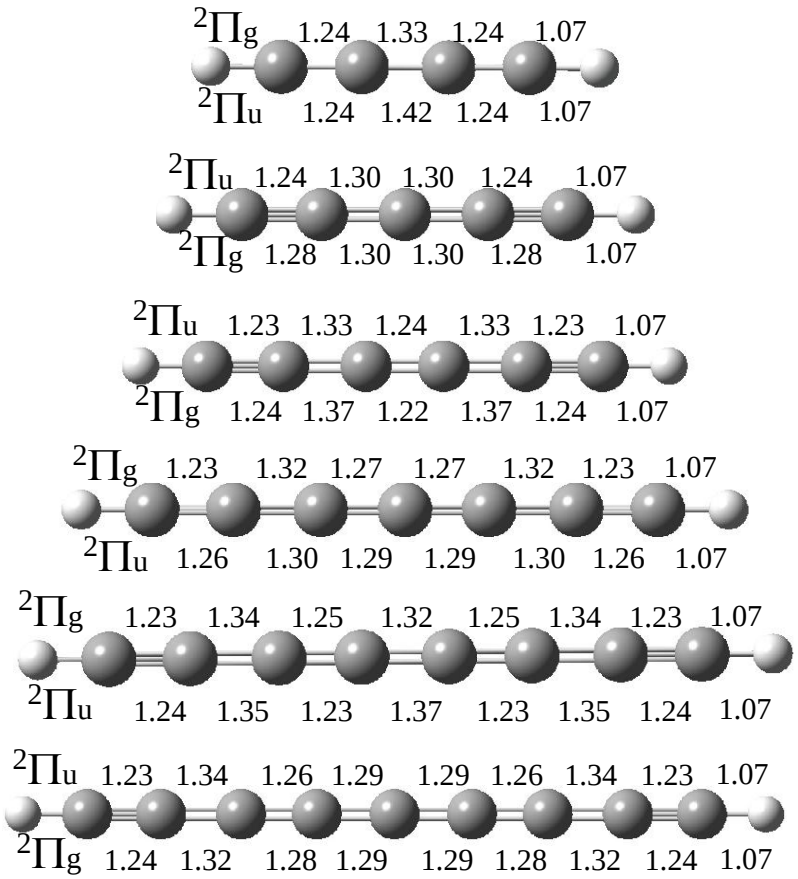

Figure S13: Optimized geometry for the two stable electronic states for linear HC_nH^+ (n = 4–9).

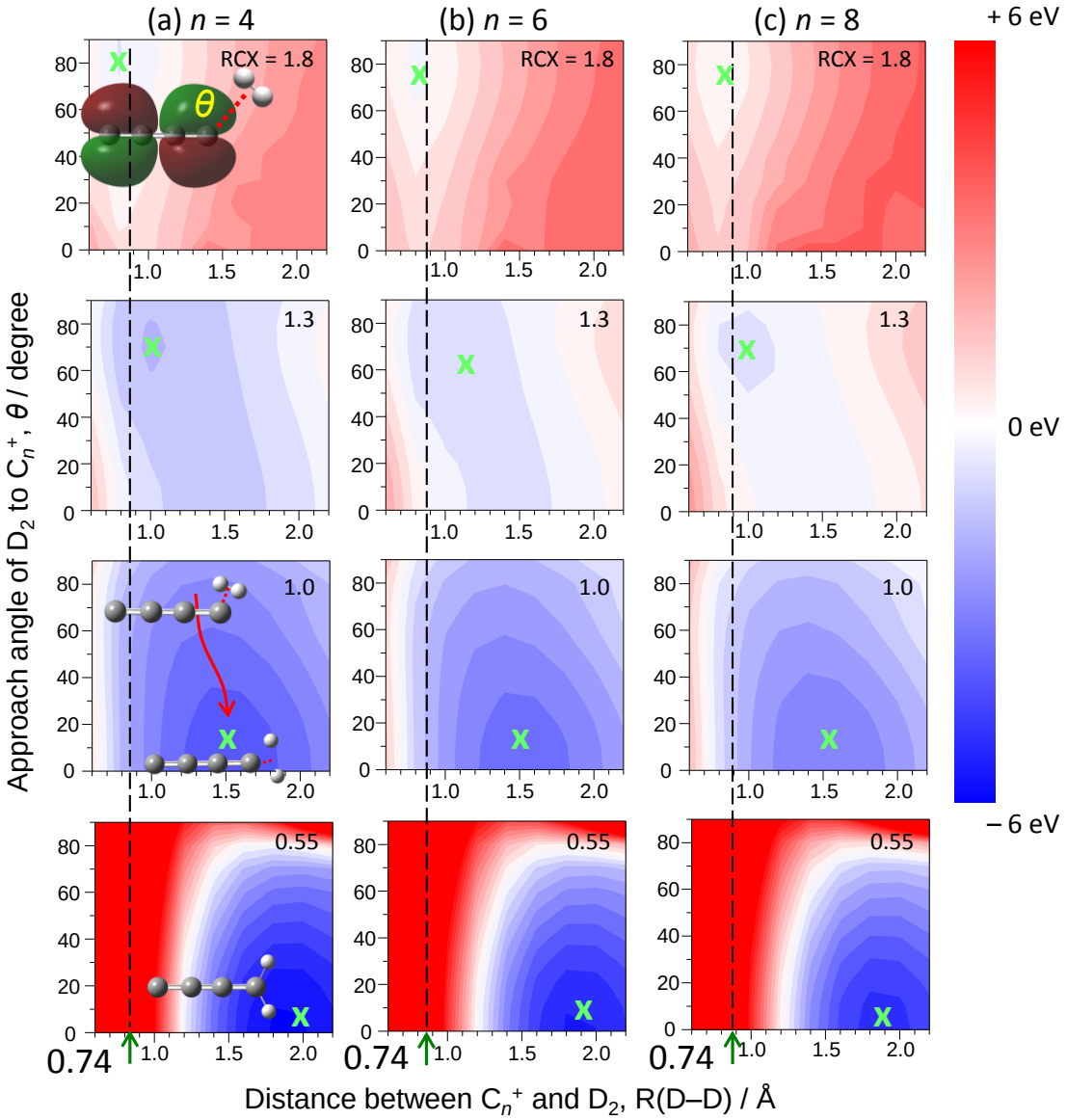

Figure S14: Potential energy surface for perpendicular approach for the D_2 addition to e ven chain (a) C_4^+ and (b) C_6^+ and (c) C_8^+ at RCX=1.8, 1.3, 1.2, and 0.55 Å calculated b y B3LYP/cc-pVTZ.

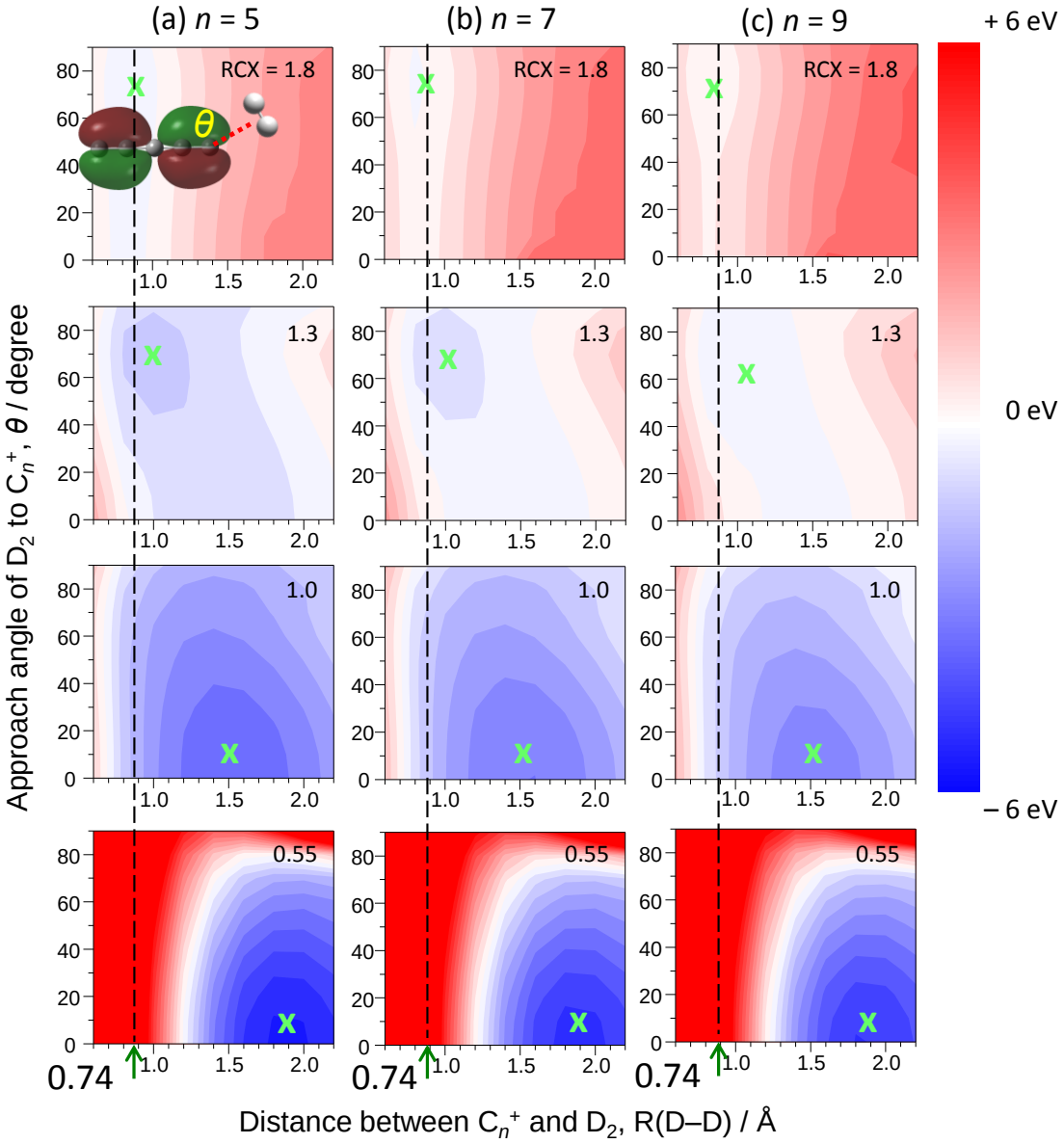

Figure S15: Potential energy surface for perpendicular approach for the D_2 addition to odd chain (a) C_5^+ and (b) C_7^+ and (c) C_9^+ at RCX=1.8, 1.3, 1.2, and 0.55 Å calculated by B3LYP/cc-pVTZ.

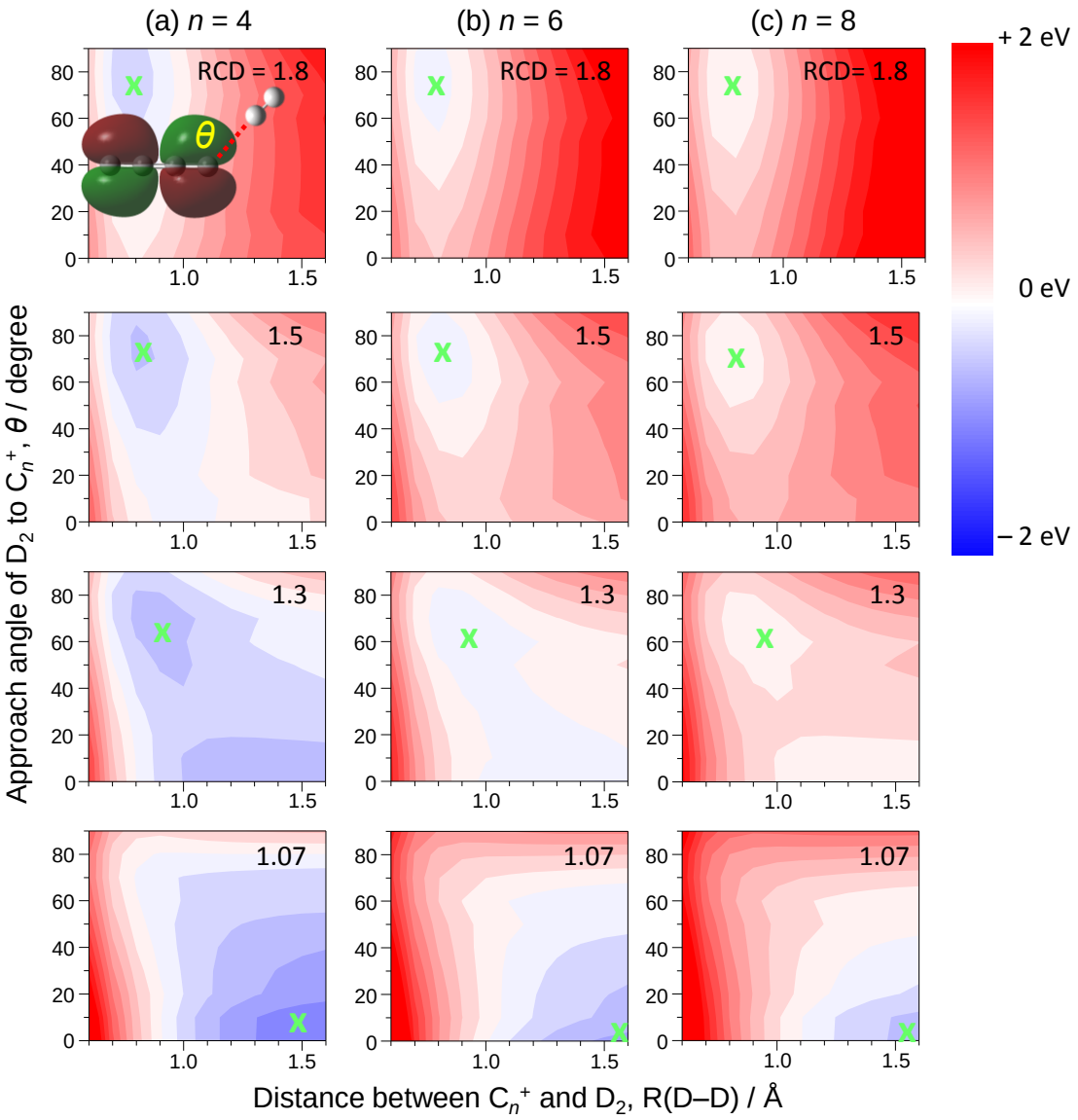

Figure S16: Potential energy surface for parallel approach for the D_2 addition to even ch ain (a) C_4^+ and (b) C_6^+ and (c) C_8^+ at RCX=1.8, 1.3, 1.2, and 0.55 Å calculated by B3L YP/cc-pVTZ.

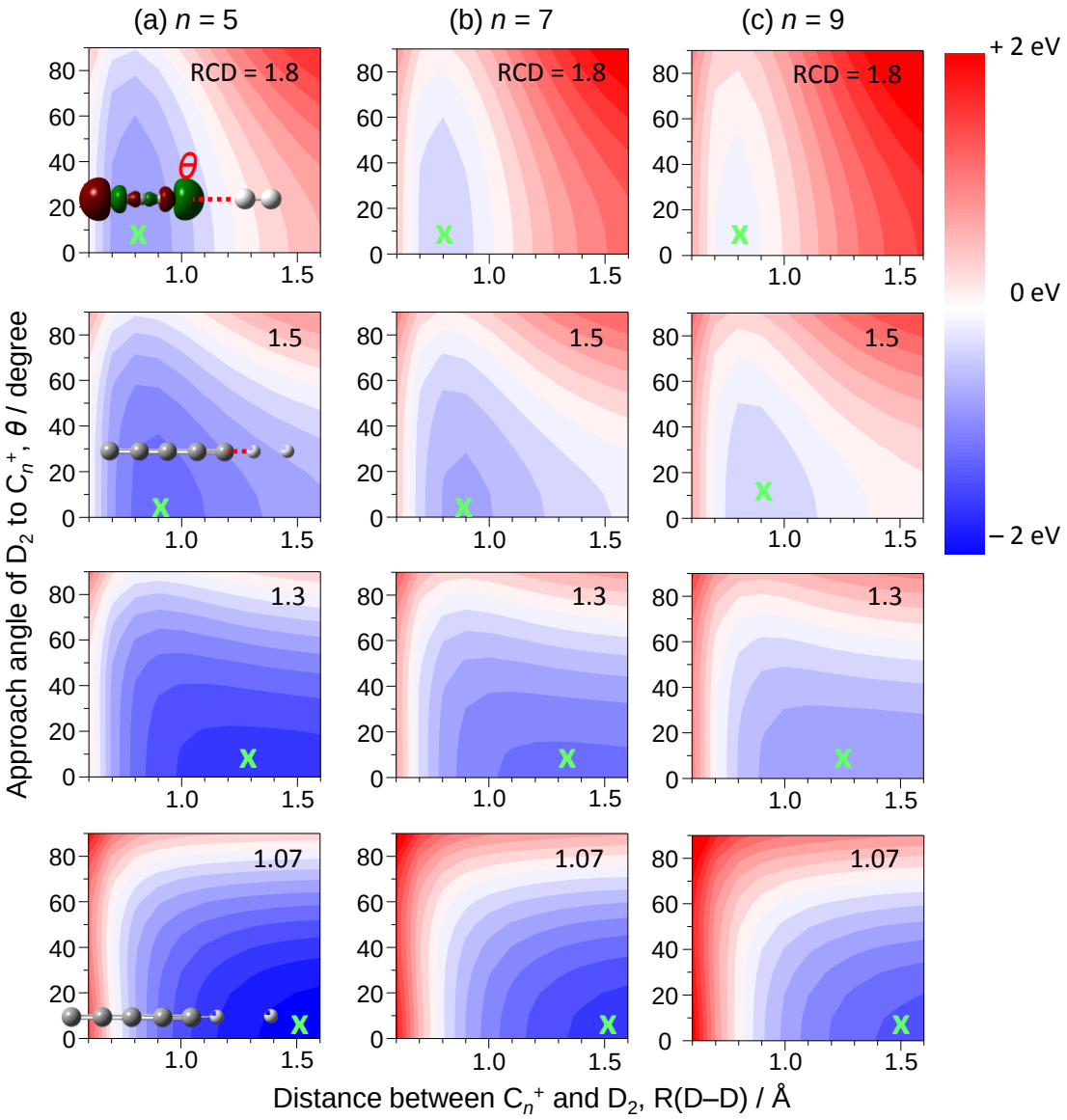

Figure S17: Potential energy surface for parallel approach for the D_2 addition to odd chain (a) C_5^+ and (b) C_7^+ and (c) C_9^+ at RCX=1.8, 1.3, 1.2, and 0.55 Å calculated by B3LYP/cc-pVTZ.

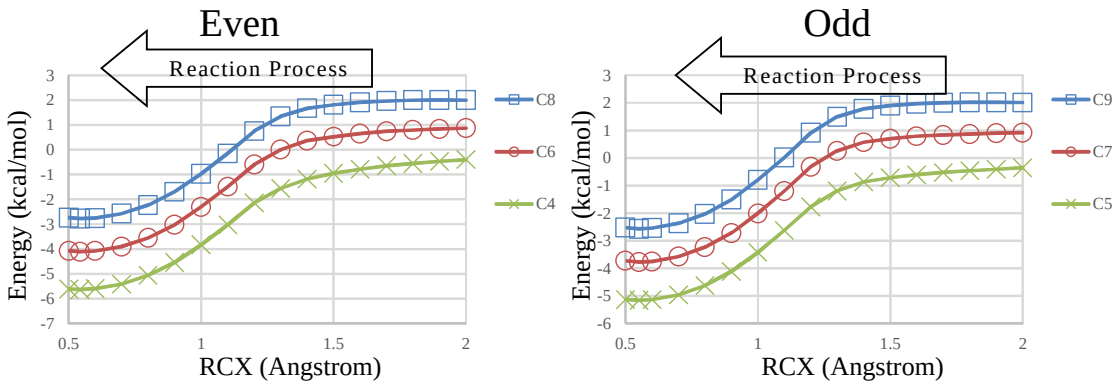

(a) Potential Energy Curve

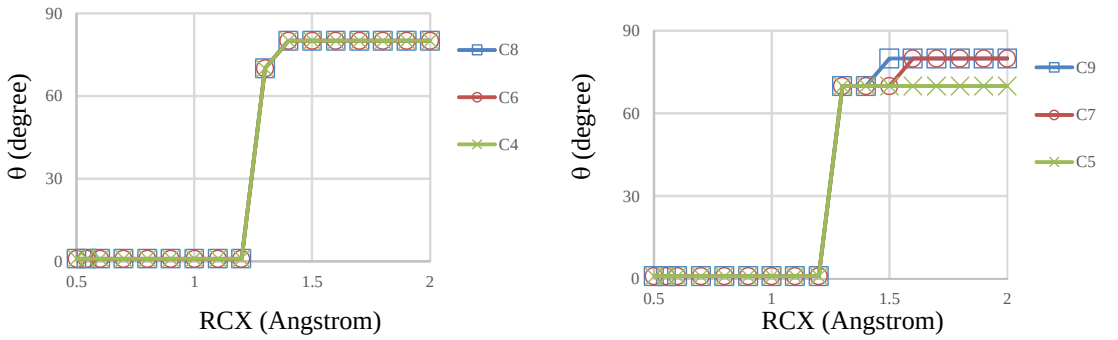

(b) Optimized θ (degree)

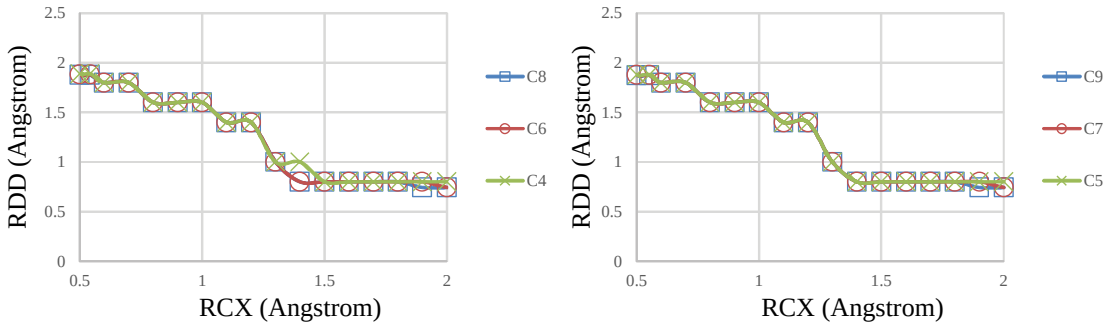

(c) Optimized RDD (Angstrom)

Figure S18: Effective potential energy curve along RCX for D_2 addition for (a) perpendicular approach to C_n^+ (n=4-9). The optimized θ angle as well as the RDD distance are given in (b) and (c) respectively.

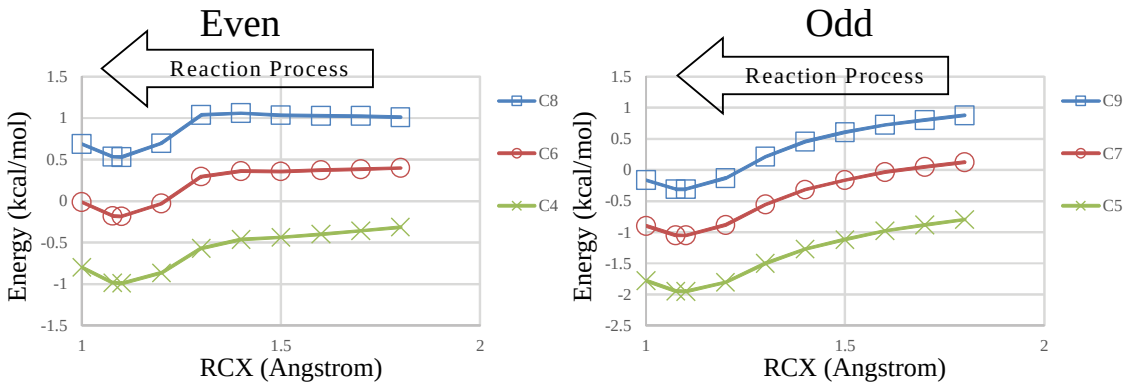

(a) Potential Energy Curve

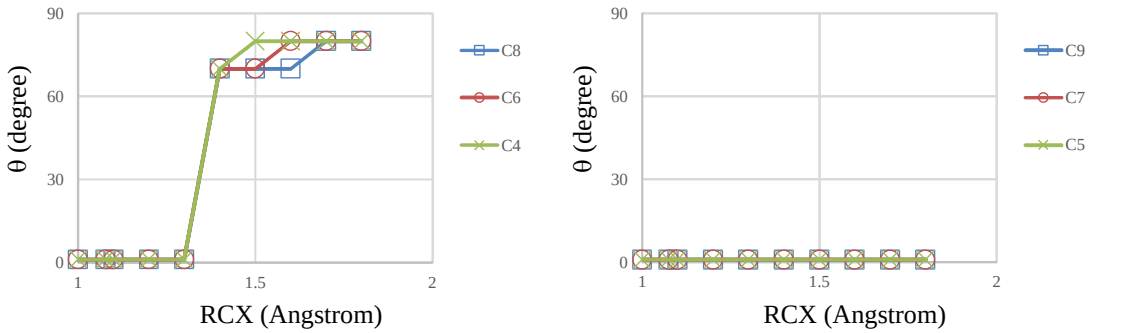

(b) Optimized θ (degree)

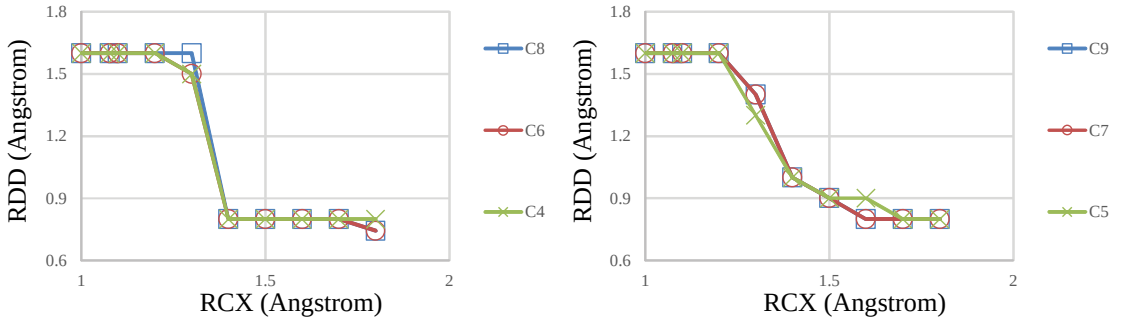

(c) Optimized RDD (Angstrom)

Figure S19: Effective potential energy curve along RCD for D_2 addition for (a) parallel approach to C_n^+ (n=4-9). The optimized θ angle as well as the RDD distance are given in (b) and (c) respectively.

Tables:

Table S1: Relative energy, in eV, of the C_n^+ in the doublet state calculated using the CCSD(T)/cc-pVTZ method. Available experimental values by Maier et al.[9] are given in parenthesis[a].

state	C_4^+	C_5^+	C_6^+	C_7^+	C_8^+	C_9^+
C_{2V} $^2\Sigma$	1.13	0.00	1.11	0.00	1.07	0.00
D_{2h} $^2\Sigma g$	1.28	0.33	1.38	0.31	1.37	0.33
D_{2h} $^2\Sigma u$	1.59	0.24	1.41	0.30	1.37 (1.39)	0.33
D_{2h} $^2\Pi u$	2.90	3.33	0.00	0.22	1.95 (1.81/2.07)	1.73
D_{2h} $^2\Pi g$	0.00	0.49	2.43 (1.92)	2.45	0.00	0.07

a: Experimental values from reference 10.

Table S2: Relative energy, in ev, of the C_n^+ in the quartet state with respect to the most stable doublet state.

state	C_4^+	C_5^+	C_6^+	C_7^+	C_8^+	C_9^+
C_{2v} $^4\Sigma$	0.13	2.16	0.57	1.82	0.54	1.60
D_{2h} $^4\Sigma g$	0.20	2.32	0.58	2.02	0.73	1.83
D_{2h} $^4\Sigma u$	0.45	2.40	0.61	2.03	0.72	1.83
D_{2h} $^4\Pi u$	0.52	2.59	3.21	1.38	1.05	1.54
D_{2h} $^4\Pi g$	3.26	5.11	0.88	1.96	3.03	1.32

Table S3: Frequency information of the linear C_n^+.

Size	Electronic State	Imaginary Frequency?	Imaginary Frequency value and mode (cm^{-1})	Largest Frequency (cm^{-1})	Symmetry (using D_{2h} for $D_{\infty h}$ and C_{2v} for $C_{\infty v}$)
C_4^+	$^2\Pi g$	N		2086.3	Ag
C_5^+	$^2\Sigma$	N		2209.7	A1
	$^2\Sigma u$	N		3651.3	B1u
	$^2\Sigma g$	N		3473.1	B1u
	$^2\Pi g$	Y	188.2, 183.7 bending	2110.5	B1u
C_6^+	$^2\Pi u$	N		2145.3	Ag
C_7^+	$^2\Sigma$	N		2200.3	A1

	$^2\Pi u$	N		2481.6	B1u
	$^2\Sigma u$	N		3401.1	B1u
	$^2\Sigma g$	Y	0.8 bending	3392.4	B1u
C_8^+	$^2\Pi g$	N		2116.1	B1u
C_9^+	$^2\Sigma$	N		2221.6	A1
	$^2\Pi g$	N		2202.1	B1u
	$^2\Sigma u$	Y	48.5 bending	3258.1	B1u
	$^2\Sigma g$	Y	59.5 bending	3257.9	B1u

Table S4: Reltaive energy, in ev, of the C_nD^+ in different spin states, the zero of energy corresponds to the most stable C_nD^+.

	C_4D^+	C_5D^+	C_6D^+	C_7D^+	C_8D^+	C_9D^+
$^1\Sigma$	0.57	0.00	0.40	0.00	0.31	0.00
$^3\Sigma$	0.00	2.45	0.00	1.52	0.00	1.75
$^3\Pi$	0.17	1.61	0.34	1.50	0.42	3.92

Table S5: Relative energy, in ev, of the $C_nD_2^+$ in different spin states, the zero of energy corresponds to the most stable $C_nD_2^+$.

	$C_4D_2^+$	$C_5D_2^+$	$C_6D_2^+$	$C_7D_2^+$	$C_8D_2^+$	$C_9D_2^+$
$^2A_1$	0.38	0.26	0.40	0.33	0.38	0.33
$^2B_1$	0.00	1.53	0.00	1.10	0.00	0.82
$^2B_2$	1.89	0.00	1.27	0.00	0.92	0.00
$^4A_1$	3.21	2.15	2.60	1.91	2.28	1.69
$^4B_1$	3.11	3.66		2.77		2.19
$^4B_2$	3.98		3.03	1.57	2.44	1.28
$^4A_2$	1.53	1.31	4.87	4.39		4.30

Table S6: Relative energy, in ev, of the DC_nD^+ in the double state, the zero of energy corresponds to the most stable $C_nD_2^+$.

	DC_4D^+	DC_5D^+	DC_6D^+	DC_7D^+	DC_8D^+	DC_9D^+
Σ_g	5.18	5.92	5.78	5.78	7.04	5.89
Σ_u	5.73	6.06	5.98	5.96	6.16	5.89

Π_u	0.83	-1.61	-1.79	0.91	-0.03	-1.86
Π_g	-1.69	1.85	0.40	-1.74	-1.92	0.63

Table S7: Vibrational peak positions in cm^{-1} and IR intensities in km/mol for the DC_4D^+ and $C_4D_2^+$ calculated using B3LYP/cc-pVTZ

DC_4D^+		$C_4D_2^+$	
Peak Position	IR Intensity	Peak Position	IR Intensity
191.1	11.8	74.8	5.4
200.5	13.9	133.4	0.4
444.5	0.0	357.3	1.0
482.3	0.0	366.9	14.0
525.2	33.2	750.9	10.9
532.2	0.0	810.7	0.7
623.9	7.7	827.6	0.2
642.4	0.0	1059.7	46.5
921.2	0.0	1492.9	142.0
1801.7	323.7	2070.8	386.3
2120.8	0.0	2234.0	87.5
2583.2	53.1	2358.8	39.8
2623.2	0.0		

Table S8: Vibrational peak positions in cm^{-1} and IR intensities in km/mol for the DC_5D^+ and $C_5D_2^+$ calculated using B3LYP/cc-pVTZ

DC_5D^+		$C_5D_2^+$	
Peak Position	IR Intensity	Peak Position	IR Intensity
120.2	9.7	72.8	5.7
127.5	10.7	113.6	0.2
280.6	0.0	215.6	12.2
345.7	0.0	251.9	6.3
393.4	29.0	393.4	2.2
410.8	11.9	559.5	5.3
415.6	0.0	722.8	0.5
572.7	18.4	776.6	0.1

675.7	0.0	798.3	9.7
681.0	1.1	1018.1	40.3
759.6	0.0	1364.3	160.0
1527.3	44.2	1859.5	50.2
1928.3	1092.7	2067.7	642.1
1949.1	0.0	2243.2	72.1
2561.8	29.3	2351.3	27.9
2595.5	0.0		

Table S9: Vibrational peak positions in cm^{-1} and IR intensities in km/mol for the DC_6D^+ and $C_6D_2^+$ calculated using B3LYP/cc-pVTZ

DC_6D^+		$C_6D_2^+$	
Peak Position	IR Intensity	Peak Position	IR Intensity
98.2	7.0	86.0	0.1
102.4	8.2	86.1	0.6
239.1	0.0	186.0	10.8
241.6	0.0	189.6	5.8
415.8	10.3	347.0	0.0
449.6	13.3	388.2	0.1
506.4	0.0	521.4	1.7
530.1	0.0	552.8	3.2
530.4	25.6	628.6	1.3
556.5	0.0	749.1	12.6
622.3	8.1	808.0	0.2
624.9	0.0	991.4	38.5
639.2	0.0	1220.7	55.7
1235.5	7.1	1624.3	127.4
1889.2	0.0	1988.8	12.4
2006.3	885.6	2116.7	1237.1
2227.5	0.0	2256.4	10.8
2613.9	2.2	2373.1	23.1
2620.2	0.0		

Table S10: Vibrational peak positions in cm-1 and IR intensities in km/mol for the DC_7D^+ and $C_7D_2^+$ calculated using B3LYP/cc-pVTZ

DC_7D^+		$C_7D_2^+$	
Peak Position	IR Intensity	Peak Position	IR Intensity
71.7	5.8	69.7	0.2
73.7	6.3	70.3	0.0
178.4	0.0	152.3	10.4
186.8	0.0	163.7	7.4
296.9	6.6	274.8	0.1
351.3	9.8	275.4	0.2
418.1	0.0	395.9	0.8
439.3	6.6	511.3	0.8
470.8	26.1	514.7	0.7
472.0	0.0	553.8	0.5
523.8	0.0	563.1	6.2
558.9	0.0	780.9	12.2
592.4	20.1	789.2	0.0
650.6	0.0	954.6	44.6
652.4	3.1	1127.3	33.9
1080.9	0.1	1501.7	79.6
1656.3	0.0	1866.4	411.6
1867.9	2263.5	1987.3	241.9
1994.2	63.5	2133.3	966.6
2059.0	0.0	2259.5	149.3
2607.9	41.6	2364.7	18.6
2616.1	0.0		

Table S11: Vibrational peak positions in cm^{-1} and IR intensities in km/mol for the DC_8D^+ and $C_8D_2^+$ calculated using B3LYP/cc-pVTZ

DC_8D^+		$C_8D_2^+$	
Peak Position	IR Intensity	Peak Position	IR Intensity
58.5	4.3	55.5	0.0
60.7	4.9	57.6	0.0
152.8	0.0	133.2	6.1
156.2	0.0	135.6	8.7
265.5	5.6	224.7	0.3
267.5	6.7	232.5	0.2

401.5	0.0	343.3	0.6
429.5	0.0	386.9	2.7
489.4	14.2	492.0	1.1
490.1	0.0	500.2	1.1
514.4	0.0	507.1	0.2
522.0	9.7	534.2	0.5
535.7	22.4	559.7	5.0
535.8	0.0	745.2	13.7
571.6	0.0	809.2	0.0
614.7	9.1	897.4	30.8
615.3	0.0	1064.7	3.9
952.5	0.5	1372.0	73.4
1390.2	0.0	1667.8	100.5
1915.5	519.1	1919.2	1008.7
2013.2	0.0	2050.4	5.5
2140.5	1318.4	2172.2	1584.1
2200.9	0.0	2264.9	14.5
2626.6	0.5	2378.6	15.7
2633.9	0.0		

Table S12: Vibrational peak positions in cm^{-1} and IR intensities in km/mol for the DC_9D^+ and $C_9D_2^+$ calculated using B3LYP/cc-pVTZ

DC_9D^+		$C_9D_2^+$	
Peak Position	IR Intensity	Peak Position	IR Intensity
45.6	3.6	46.0	0.0
47.4	3.9	46.7	0.0
121.4	0.0	114.2	7.1
123.3	0.0	115.2	6.0
214.9	4.7	194.7	1.0
223.7	6.3	199.0	0.3
306.2	0.0	289.4	2.5
352.9	0.0	297.2	2.4
414.8	8.0	390.7	0.3
441.9	0.0	443.1	0.4
457.5	0.0	483.8	0.4
462.6	5.6	491.6	0.1
494.1	4.7	527.6	0.3
499.0	25.3	540.5	0.6

499.3	0.0	559.3	6.3
555.2	0.0	768.7	13.8
591.7	19.0	795.8	0.0
631.5	0.0	833.7	27.5
631.5	5.4	1029.8	1.9
859.7	6.8	1266.3	40.3
1257.5	0.0	1579.9	208.2
1713.6	532.7	1848.5	96.1
1814.5	3483.5	1904.7	1083.0
1969.9	0.0	2093.4	176.1
2058.5	111.5	2172.9	1647.3
2137.8	0.0	2266.5	102.5
2630.8	46.5	2370.9	13.4
2631.2	0.0		

Table S13: Dissociation energies in eV for the C, C_2 and C_3-loss channels for C_nD^+ and $C_nD_2^+$.

	C loss	C_2 loss	C_3 loss
C_4D^+			
C_5D^+	7.72		
C_6D^+	5.39	7.07	
C_7D^+	7.33	6.68	7.07
C_8D^+	5.44	6.73	4.80
C_9D^+	7.11	6.51	6.52
$C_4D_2^+$			
$C_5D_2^+$	6.32		
$C_6D_2^+$	6.48	6.77	
$C_7D_2^+$	6.22	6.67	5.67
$C_8D_2^+$	6.33	6.52	5.68
$C_9D_2^+$	6.17	6.47	5.37

References

[1] E. A. Mason, and E. W. MacDaniel, *Transport Properties of Ions in Gases*, Wiley, NY, 1988.

[2] M. Schnell, M. Muhlhauser, G. E. Froudakis, and S. D. Pyerimhoff, *Chem. Phys. Lett.*, 2001, **340**, 559-564.

[3] R. S. Mulliken, *Phys. Rev.* 1939, **56**, 778-781.

[4] K. S. Pitzer, E. Clementi, *J. Am. Chem. Soc.* 1959, **81**, 4477-4485.

[5] W. D. Allen, D. A.Horner, R. L.Dekock, R. B. Remingto, and H. F. Schaefer III, *Chem. Phys.* 1989, **113**, 11-45. E. R. Davidson W. T. Borden, *J. Phys. Chem*, 1983, **87**, 4783-4790. T. D. Crawford, J. F. Stanton, W. D. Allen and H. F. Schaefer III, *J. Chem. Phys.* 1997, **107**, 10626-10632. M. L. Leininger, C. D. Sherril. W. D. Allen. and H. F. Schaefer III, *J. Chem. Phys*. 1998, **108**, 6717-6724. C. D. Sherril, M. S. Lee, and M. Head-Gordon, *Chem. Phys. Lett.* 1999, **302**, 425-430. W. Eisfeld and K. Morokuma, *J. Chem. Phys*. 2000, **113**, 5587-5597. O. Goscinski, *Int. J. Quantum Chem. Quant Chem Sympo.* 1986, **19**, 51-59. L. Engelbrecht, and B. Liu, *J. Chem. Phys.* 1983, **78**, 3097-3106. A. D. McLean, B. H. Lengsfield III, J. Pacansky, and Y. Ellinger, *J. Chem. Phys.* 1985, **83**, 3567-3576. S. Sen, P. Seal, and S. Charkrabarti, *Phys Rev. B* 2006, **73**, 245401. T. Torelli, and L. Mitas, *Phys. Rev. Lett.* 2000, **85**, 1702. N. J. Russ, T. D. Crawford, and G.S. Tschumper, *J. Chem. Phys.* 2004, **120**, 7298-7306.

[6] M. G. Guiffreda, M. S. Deleuze, J. F. Francois, *J. Phys. Chem. A* 1999, **103**, 5137-515.

[7] G. Orlova, and J. D. Goddard, *Chem. Phys. Lett.* 2002, **363**, 486-491.

[8] L. Belau, S. E. Wheeler, B. W. Ticknor, M. Ahmed, S. R. Leione, W. D. Allen, H. F. Schaefer III, M. A. Duncan, *J. Am. Chem. Soc.* 2007, **129**, 10229-10243.

[9] R. F. W. Bader, *Atoms in Molecules. A Quantum Theory*; Oxofrd University Press: New York, 1990.

[10] P. Freivogel, J. Fulara, D. Lessen, D. Forney, J. P. Maier, *Chem. Phys.* 1994, **189**, 335-341. J. P. Maier, *J. Phys. Chem. A*, 1998, **102**, 3462-3469. J. Fulara, E. Riaplov, A. Batalov, I. Shnitko, J. P. Maier, *J. Chem. Phys.* 2004, **120**, 7520. J. Fulara, I. Shnitko, A. Batalov, J. P. Maier, *J. Chem. Phys.* 2005, **123**, 044305.